

Journal Pre-proof

Soft Body Impact on Composites: Delamination experiments and Advanced Numerical Modelling

Jagan Selvaraj, Luiz F. Kawashita, Mehdi Yasaee, Gordon Kalwak, Stephen R. Hallett



PII: S0266-3538(21)00133-0

DOI: <https://doi.org/10.1016/j.compscitech.2021.108777>

Reference: CSTE 108777

To appear in: *Composites Science and Technology*

Received Date: 20 August 2020

Revised Date: 2 March 2021

Accepted Date: 15 March 2021

Please cite this article as: Selvaraj J, Kawashita LF, Yasaee M, Kalwak G, Hallett SR, Soft Body Impact on Composites: Delamination experiments and Advanced Numerical Modelling, *Composites Science and Technology*, <https://doi.org/10.1016/j.compscitech.2021.108777>.

This is a PDF file of an article that has undergone enhancements after acceptance, such as the addition of a cover page and metadata, and formatting for readability, but it is not yet the definitive version of record. This version will undergo additional copyediting, typesetting and review before it is published in its final form, but we are providing this version to give early visibility of the article. Please note that, during the production process, errors may be discovered which could affect the content, and all legal disclaimers that apply to the journal pertain.

© 2021 Elsevier Ltd. All rights reserved.

Soft Body Impact on Composites : Delamination experiments and Advanced Numerical Modelling

Jagan Selvaraj^a, Luiz F. Kawashita^a, Mehdi Yasaei^b, Gordon Kalwak^{c,d},
Stephen R. Hallett^a

^a*Bristol Composite Institute (ACCIS), University of Bristol, Queen's Building, University Walk,
Bristol BS8 1TR, UK*

^b*School of Aerospace, Transport and Manufacturing, Cranfield University, MK43 0AL, UK*

^c*Department of Engineering Science, University of Oxford, Oxford, UK*

^d*Rolls-Royce plc, Derby, UK*

Abstract

Cohesive interface elements have become commonly used for modelling composites delamination. However, a limitation of this technique is the fine mesh size required. Here, a novel cohesive element formulation is proposed and demonstrated for modelling the numerical cohesive zone with equal fidelity but fewer elements in comparison to a linear cohesive element formulation. The newly proposed formulation has additional degrees of freedom in the form of nodal rotations which when combined with the use of multiple integration points per cohesive element, allows for delamination propagation to be modelled with increased stability. This element formulation is introduced with an adaptive modelling method, termed Adaptive Mesh Segmentation (AMS). To demonstrate its effectiveness under impact loading the new model is applied to a soft body beam bending test. This test, containing a delamination pre-crack, uses inertial constraints and results in a dynamic stress state when impacted by a gelatin cylinder.

Keywords: Impact behaviour, Delamination, Finite element analysis (FEA), Cohesive element formulation

26 1. Introduction

27 The superior specific strength and stiffness provided by laminated composite struc-
28 tures allows for the design of energy efficient aerospace components. During the
29 service life, they are subjected to various loading conditions including low velocity
30 (tool drops during maintenance) and high velocity impact (strike of debris or other
31 foreign objects). High interlaminar stress can be induced by dynamic events such
32 as impact [1, 2], with delamination being one of the most critical failure phenomena
33 [3], usually accompanied by matrix cracking and ultimately fibre failure. Hence, in
34 the design of composite structures, understanding damage and the resulting loss of
35 stiffness is of vital importance. Numerical modelling of such events is generally per-
36 formed using an energy based approach that can produce mesh independent results.
37 Cohesive zone modelling (CZM) has become the preferred numerical technique to
38 characterise delamination behaviour in composite structures [4, 5, 6, 7]. CZM is
39 characterised by the presence of two constitutive relations: (i) a constitutive relation
40 for stress and strain in the continuum and (ii) a cohesive relation that for traction
41 and separation across a discontinuity.

42 A limiting requirement to discretise the numerical cohesive zone with multiple inte-
43 gration points results in a highly refined mesh when modelled with linear elements.
44 Different strategies have been adopted in the existing literature to allow for compu-
45 tations with coarser meshes.

46 Artificial interface strength reduction has been used along with linear elements to
47 increase the length of numerical cohesive zone when a coarser mesh is used [6].

48 **Although this improves the discretisation requirement, the accuracy of the method**
49 **is limited** and demonstrated with benchmark cases by Harper and Hallett [8].

50 In addition to CZM, as used in the current work, delamination modelling can also

51 be performed using the Virtual crack closure Technique (VCCT) [9] and Continuum
52 Damage Mechanics (CDM) [10]. VCCT assumes that the energy released ΔE_1 during
53 the extension of a crack by Δa is identical to the energy required to close to the crack
54 ΔE_2 . The crack or delamination progression is further determined by comparing
55 against the critical energy release rate [11]. However, VCCT requires the presence
56 of an existing crack. Unlike CZM and VCCT, CDM does not model discrete cracks.
57 The damage onset is typically calculated using a stress-based criterion; the damage
58 progression is modelled with an energy-regularised criterion. The damage calculated
59 by CDM models degrades the properties of whole element or ply [10] and hence it is
60 not suited for modelling discrete cracks and large crack opening displacements.
61 Modelling discontinuities by explicitly forming the crack surfaces within an existing
62 mesh are performed using discrete crack models. They are classified, based on the
63 enrichment method used to introduce discontinuities, into two categories, (i) meth-
64 ods that model discontinuities with the enrichment obtained from additional shape
65 functions [12, 13] and (ii) methods that use standard shape functions in order to sim-
66 plify the implementation in a commercial FE software [14, 15, 16]. However, many
67 of the existing methods use an implicit time integration scheme.
68 To obtain the structural response following impact, the impact event and the subse-
69 quent propagation of waves must be accurately modelled. The impact event causes
70 an instantaneous change in the velocity and a step change in the solution behaviour
71 - an ill-posed problem. It induces high frequency waves in the material and requires
72 a small time step to study that wave. Hence, an explicit time integration scheme is
73 required [17]. In explicit methods, the global time step is calculated based on element
74 time steps; if the above mentioned methods to model discontinuities are used, split-
75 ting of elements following the formation of crack surfaces will result in the subsequent
76 reduction of element time steps and hence the global time step. Such a scenario will

77 be computationally very expensive in the analysis of structural components. Also,
78 mapping of information to the newly created elements can cause numerical oscilla-
79 tions. Hence, a method that models discontinuities without reducing the time step,
80 while allowing coarser meshes, is required, in particular for impact loading.

81 A novel cohesive element which uses coordinate rotations has been proposed to en-
82 hance the mesh size capability over linear elements [18]. The additional rotational
83 degrees of freedom, coordinate rotations, allow for modelling of displacement across
84 the crack surfaces with C^1 continuity, providing improved resolution in the numerical
85 cohesive zone. These additional degrees of freedom present at the location of nodes
86 makes it compatible with existing 8 noded meshes and this results in fewer degrees
87 of freedom than a quadratic cohesive element formulation which requires 20 noded
88 meshes. Furthermore, multiple integration points can be employed within a cohesive
89 element **improving the discretisation of numerical cohesive zone length. Since the**
90 **spacing of integration points is smaller than linear elements at a given mesh size,**
91 **stable crack propagation is possible even when using coarser mesh sizes. Hence, ac-**
92 **curate results can be obtained with rotation enabled cohesive segments and this is**
93 **described with numerical examples in [18].**

94 In the current work, this novel cohesive element formulation is applied to the challeng-
95 ing case of a soft body impact and shown to perform well in regards to delamination
96 predictions and also computational efficiency.

97 Adaptive Mesh Segmentation (AMS) [19] based on a ‘simplified cohesive segment’
98 [16] may offer a possible solution to maintain a constant global time step and to
99 avoid numerical oscillations. This method enables automatic insertion of cohesive
100 elements, at element boundaries, to maintain a constant time step size following crack
101 initiation. Moreover, a traction vector calculated from the element nodal forces is
102 also included in the AMS method to increase compatibility with the surrounding

103 stress field and minimise residuals associated with the initiation. Although methods
104 have been suggested in the past to smear the residuals [20], minimisation of such
105 errors in explicit time integration is an integral feature of this method.

106 Experimental methods such as three point bend tests along with impact loading are
107 commonly used to understand delamination initiation and progression in composite
108 specimens [21, 22]. Following impact, matrix cracks originates around the location
109 of impact and the ends of the beam which is followed by delamination. The effects
110 of boundary conditions are unavoidable. In order to create representative damage
111 events following a soft body impact on aerospace components, the soft body beam
112 bending (SBBB) test was invented [23]. The SBBB test is a modified three point
113 bend test which uses inertial boundary conditions and so avoids unwanted failures at
114 these locations. The impact triggers through thickness shear loading around the site
115 of impact followed by a bending response in the beam, which can change in curvature
116 depending on the initial impact velocity and inertial constraints.

117 **2. Soft Body Beam Bend Test - Experiments**

118 The Soft Body Beam Bend (SBBB) test [23] is a modified three point beam bending
119 test, in which the beam is suspended from above, with low rotational inertia fittings
120 clamped on the beam ends to provide inertial restraint to translational movement
121 whilst avoiding localised stress and unrealistic failure of the specimen The SBBB
122 aims to replicate the dynamic stress state that occurs following impact on an in-
123 service composite component. The objectives of this experimental method are (i)
124 to determine the threshold velocity, which is defined as the velocity at which full
125 delamination is obtained along the length of a specimen, (ii) to determine the effec-
126 tiveness of through thickness reinforcements [24] and (iii) to provide experimental

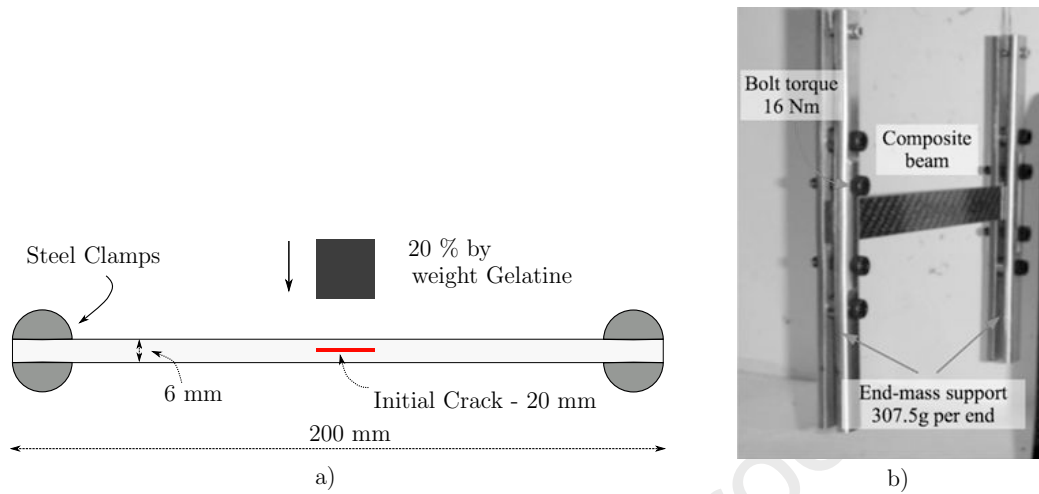


Figure 1: a) Schematics of the SBBB test setup; all specimens have a width of 20 mm. b) Experimental setup.

127 results with a pre-defined set up that can be replicated in numerical models and
 128 analyse the influence of material parameters.

129 The schematics of the SBBB test and the specimen dimensions are shown in Figure 1.
 130 The specimen is fastened to the steel end clamps with a torque of 16 N·m, which are
 131 then suspended from long cables. The time period of the system can be varied by
 132 adjusting the mass of the clamps, *i.e.* an increase in the mass of the clamps results
 133 in the time period of the clamps being higher than the system and the composite
 134 specimen. This will force a change in the curvature of the specimen when subjected
 135 to impact, changing the resulting concavity of the specimen.

136 Composite specimens manufactured from carbon fibre epoxy material (IM7/8552)
 137 were used in the current work. A symmetric, balanced layup sequence of ((0,-
 138 45, 0, 45)_{3S})_S was used, with a total laminate thickness of 6 mm. A pre-crack of length
 139 20 mm was manufactured into the specimens at their mid-planes, using 5m thick
 140 metal shim material [25]. Under impact loading the delamination growth originates

141 from the pre-crack tip and grows away from the impact location. Ballistic gelatine
142 (20% by weight) is used for the impactor material. The impactor was cylindrical in
143 shape with length and diameter 20 mm, and a mass of 6.5 g.

144 **3. Modelling Details**

145 *3.1. Cohesive Elements with Rotations*

146 In linear cohesive elements with four integration points, a crack can traverse the en-
147 tire element length in a single time increment when the energy release rate associated
148 with an integration point exceeds the fracture energy. In order to avoid numerical
149 instabilities associated with the rate of crack growth, and to provide sufficient reso-
150 lution of the numerical cohesive zone bridging forces, an alternative cohesive element
151 formulation is required.

152 The proposed cohesive element results in a reduction in the area associated with an
153 integration point by allowing the presence of multiple integration points and crack
154 traverses the cohesive element in a finite time.

155 It should be noted that increasing the number of integration points in a linear cohe-
156 sive segment does not result in a change in the order of continuity and so the new
157 formulation is augmented with additional degrees of freedom. Full details of the new
158 element formulation are given in [18] and so only the essential features are recounted
159 briefly here.

160 The non-linear displacement field can be represented by two different configurations:
161 (i) with additional rotational degrees of freedom at the corner nodes or, (ii) by
162 inserting virtual mid-side nodes and calculating their equivalent displacement. The
163 first configuration is used in the calculation of cohesive forces from cohesive tractions
164 while the second is used in the evaluation of this traction vector from the cohesive law,

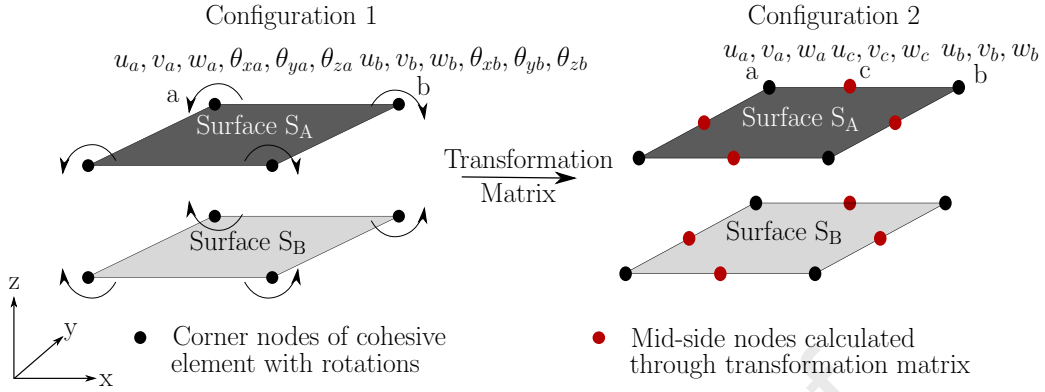


Figure 2: Kinematics in a cohesive segment.

165 since it is described only using translations. The two configurations are graphically
 166 shown in Figure 2. The calculation of equivalent displacement in one of the mid side
 167 nodes, c is obtained from the corner nodes a and b by,

$$u_c = \frac{(u_a + u_b)}{2} + \frac{y_b - y_a}{8}(\theta_{zb} - \theta_{za}) + \frac{z_b - z_a}{8}(\theta_{ya} - \theta_{yb}) \quad (1)$$

$$v_c = \frac{(v_a + v_b)}{2} + \frac{z_b - z_a}{8}(\theta_{xb} - \theta_{xa}) + \frac{x_b - x_a}{8}(\theta_{za} - \theta_{zb}) \quad (2)$$

$$w_c = \frac{(w_a + w_b)}{2} + \frac{x_b - x_a}{8}(\theta_{yb} - \theta_{ya}) + \frac{y_b - y_a}{8}(\theta_{xa} - \theta_{xb}) \quad (3)$$

168 where x, y, z are cartesian coordinates, u, v, w are translation degrees of freedom, and
 169 $\theta_x, \theta_y, \theta_z$ are rotation degrees of freedom.

170 If equations (1) to (3) are written in matrix form for all nodes, it would represent
 171 a matrix that maps the displacement field between the two configurations and the
 172 transformation matrix \mathbf{T}_{coh} is given by,

$$\mathbf{U}_{\text{quad}} = \mathbf{T}_{\text{coh}} \mathbf{U}_{\text{rot}} \quad (4)$$

173 where \mathbf{U}_{rot} is the displacement vector defined in terms of translations and rotations
 174 (Configuration 1) and \mathbf{U}_{quad} is the displacement vector defined only in terms of

175 translations (Configuration 2). The dimension of \mathbf{T}_{coh} is 48×48 . At any given time
 176 increment, \mathbf{U}_{quad} and \mathbf{U}_{rot} represents the same displacement field.
 177 To interpolate the displacement in the configuration 2, quadratic shape functions,
 178 \mathbf{N}_{quad} , of a two-dimensional element is assembled from both the surfaces of a cohesive
 179 element. For configuration 1, new shape functions need to be derived from \mathbf{N}_{quad}
 180 using \mathbf{T}_{coh} of the cohesive element by,

$$\mathbf{N}_{\text{rot}} = \mathbf{N}_{\text{quad}} \mathbf{T}_{\text{coh}} \quad (5)$$

181 where \mathbf{N}_{rot} is the shape function to interpolate the displacements in configuration 1.
 182 The displacement vector, $\boldsymbol{\delta}$, at multiple integration points can be interpolated from
 183 \mathbf{U}_{quad} using quadratic shape functions, \mathbf{N}_{quad} . The traction vector, $\boldsymbol{\tau}$, is then
 184 calculated using a cohesive law. In the current work, a bi-linear traction separation
 185 law [5] developed at the University of Bristol is used to model the crack initiation
 186 and propagation defined by an energy criterion.

187 3.2. Higher Order AMS

188 Insertion of cohesive elements in a finite element mesh before the start of an analy-
 189 sis requires significant effort and introduces a finite stiffness between the continuum
 190 elements. This can alter the compliance of an undamaged structure [7] and also the
 191 manner and speed with which dynamic stress waves propagate through it. With
 192 Higher order Adaptive Mesh Segmentation (AMS), the insertion of the proposed co-
 193 hesive elements is performed ‘on-the-fly’ *i.e.* the displacement discontinuities in the
 194 out-of-plane direction are modelled by introducing cohesive behaviour between the
 195 continuum elements according to a physically based criterion and without user inter-
 196 vention. The Higher order AMS is implemented as a user element in the commercial
 197 finite element software LS-DYNA. The new element formulation contains both the

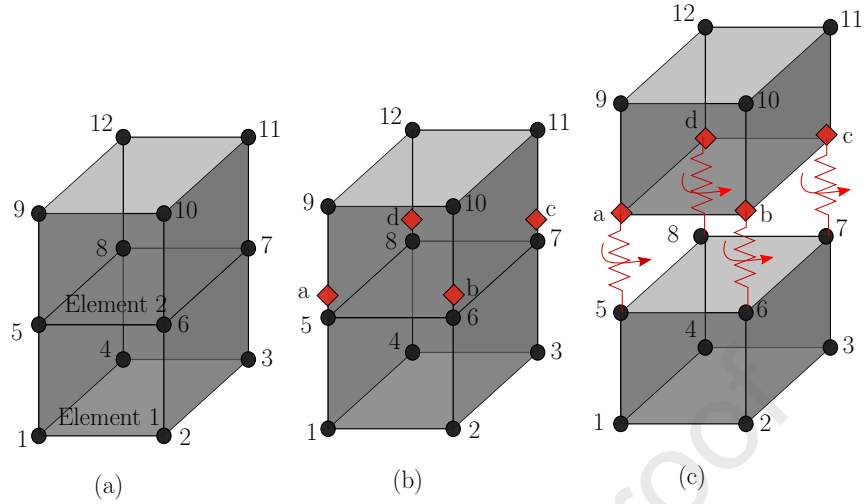


Figure 3: Element segmentation operation, (a) Global numbering of nodes before segmentation at $t < t_s$; (b) At the time of segmentation, new nodes are initiated from the location of existing nodes by mapping field and state variables at $t = t_s$; (c) Cohesive elements with rotations are initiated after segmentation at $t > t_s$.

198 continuum element formulation and the cohesive element formulation described in
 199 Section 3.1.

200 A compatible continuum element formulation [26], 8 node hexahedral elements with
 201 nodal rotations (48 DOF), is used as the continuum element in Higher order AMS.
 202 To define the mass matrix for the additional degrees of freedom, rotational inertia
 203 is used. A multiplicative factor (α) is used with the rotational inertia to obtain a
 204 stable time step while not affecting the global behaviour of the numerical model. This
 205 continuum element [26] is also available as a built-in library element in LS-DYNA as
 206 ELFORM = 3.

207 Different stages of segmentation are shown schematically in Figure 3. An element is
 208 selected for segmentation upon reaching a segmentation initiation criterion based on
 209 the stress tensor at time t_s . New nodes (a,b,c,d), shown in Figure 3b, are initiated

210 from the location of existing nodes. Existing element connectivity in LS-DYNA
211 cannot be updated. Hence, the element connectivity is updated with the new nodes
212 and time integration of these new nodes is performed at the end of every increment
213 within the user subroutine. State variables of the new nodes, available only within
214 the user subroutine, can be visualised by writing additional output files. Cohesive
215 segments are initiated based on the updated connectivity as shown in Figure 3c;
216 the red coloured nodes and the cohesive segments belong internally within the user
217 subroutine. Also, these cohesive segments are initiated a traction vector, compatible
218 with the surrounding stress field to prevent the introduction of numerical errors.
219 Standard elements from LS-DYNA (ELFORM = 3) are used in the regions of mesh
220 where delamination is not expected to initiate and also the computational times of
221 built-in library elements are faster. Hence, Higher order AMS can be used along
222 with this LS-DYNA library element in delamination modelling.

223 *3.3. Impactor modelling*

224 A soft body (or gelatine) displays fluid-like behaviour when impacting a stiffer target
225 material, such as carbon-fibre reinforced polymer material. Therefore, to model the
226 soft body impact and its hydrodynamic response, Smooth Particle Hydrodynamics
227 (SPH) is used. SPH also avoids instabilities associated with Lagrangian meshes
228 undergoing severe element distortion.

229 The pressure-volume behaviour is described through equation of state (EOS). The
230 EOS parameters are derived from Hugoniot impact tests for 20 % gelatine by weight
231 [27]. The shock velocity, U_s , is related to the particle velocity, U_p , by

$$U_s = 1.57 + 1.77 U_p. \quad (6)$$

232 This is implemented in LS-DYNA via keyword *EOS_LINEAR_POLYNOMIAL
233 with corresponding constants ($c_0 = 0; c_1 = 2613; c_2 = 6637; c_3 = 8671$). Material

234 card *MAT_NULL is also used to model the volumetric behaviour of the impactor
235 with a negative cut-off pressure.

236 3.4. Continuum modelling

237 The material properties used for numerical analysis of the SBBB test are shown in
238 Table 1. The key elastic modulus for the test coupon behaviour is the fibre direction
239 modulus, E_{11} , since the layup is unidirectional and the main deformation mode is
240 bending. For carbon-fibre, fibre direction properties are generally not considered to
241 be rate dependent [28, 29]. The transverse matrix dominated modulus E_{22} , that
242 might be expected to be more rate dependent, does not affect the bending defor-
243 mation here. This assumption to neglect strain rate dependency does not cause a
244 significant influence in the model formations and this is explained in Section 4.1.

245 In the cohesive law, fracture energy is the governing parameter for modelling de-
246 lamination progression in the case of a pre-crack, as is used here. Rate dependence
247 of the initiation stresses can thus be ignored. For IM7/8552, strain rate dependent
248 3-ENF Mode II tests revealed that the fracture energy is 0.97 N/mm [30] for high
249 strain rate cases and 0.2 N/mm for Mode I fracture energy in high strain rate tests
250 using DCB specimens [31]. Similar values are used in the current work.

251 The composite layup is homogenised with twelve elements of size 0.5 mm in the
252 through-thickness direction. The mesh size used for the in-plane direction of the
253 specimen is 1 mm; this mesh size was chosen based on quasi-static tests from [18] and
254 a detailed analysis on mesh sizes is shown in Section 4.3. Similar to the experiments
255 a pre-crack of length 20 mm is modelled by using cohesive elements of negligible
256 interface strength and fracture energy. The penalty stiffness helps to avoid the inter-
257 penetration of elements. The model setup is shown in Figure 7a. Matrix cracks
258 are assumed to have negligible influence on the impact-driven delamination crack

Table 1: Material parameters for IM7/8552 used in benchmark cases

E_{11} (GPa)	$E_{22} = E_{33}$ (GPa)	$G_{12} = G_{13}$ (GPa)	G_{23} (GPa)	$\nu_{12} = \nu_{13}$	ν_{23}
161	11.38	5.17	3.98	0.32	0.43
G_{Ic} (N/mm)	G_{IIc} (N/mm)	$\sigma_{I,max}$ (MPa)	$\sigma_{II,max}$ (MPa)	K_I (N/mm ³)	K_{II} (N/mm ³)
0.2	1.0	60.0	90.0	10 ⁴	10 ⁴

259 propagation and so are ignored in the current numerical model.

260 4. Results and Discussion

261 4.1. SBBB Model Validation

262 The numerical model is initially validated for displacement time history via high
 263 speed video from experiments, in order to test the ability of the model to represent
 264 physical specimen behaviour. Higher order AMS is assigned to the row of elements
 265 located near the pre-crack region and therefore where delamination is expected to
 266 initiate (green zone in the model in Figure 7). The rest of the laminate is modelled
 267 with elements of compatible degrees of freedom, 8-node hexahedral elements with
 268 nodal rotations, available as (ELFORM - 3) in LS-DYNA (red zone in the model in
 269 Figure 7).

270 Linear and quadratic bulk viscosity values of 0.06 and 1.5 were used in numerical
 271 models. Finally, analysis was conducted over 2.5 ms.

272 Figure 4 shows the displacement *vs.* time curve at the specimen centre-line for
 273 the experiment and Higher order AMS for the impact velocity of 88 m/s. It can
 274 be observed that the displacement history of Higher order AMS at the point of
 275 impact compares well with experimental results. The numerical model using higher

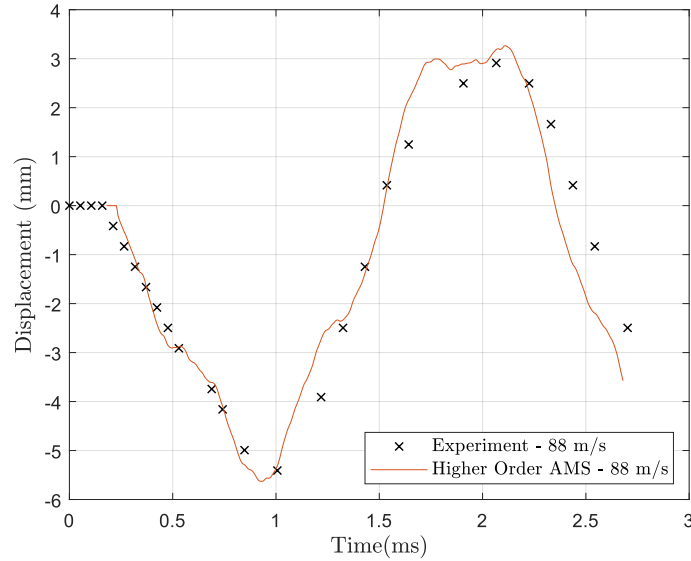


Figure 4: Comparison of centre-line displacement-time history obtained for a projectile with an initial velocity of 88 m/s.

276 order AMS captures the maximum displacement in both the positive and negative
 277 curvature of bending. Also, the assumption to neglect strain rate dependency does
 278 not cause a significant influence in model deformations. Impact loading creates a
 279 change in curvature locally in the proximity of the impact zone, before the entire
 280 specimen is subjected to bending.

281 4.2. Threshold Velocity

282 The proposed cohesive element formulation is used to perform threshold velocity
 283 calculations in this section. Minor changes in the location of impact can cause
 284 considerable change in the delamination growth for a given impact velocity. As such,
 285 it is critical to understand the actual location of impact from experiments. In this
 286 context, the results are presented in two different sections: (i) a section where the

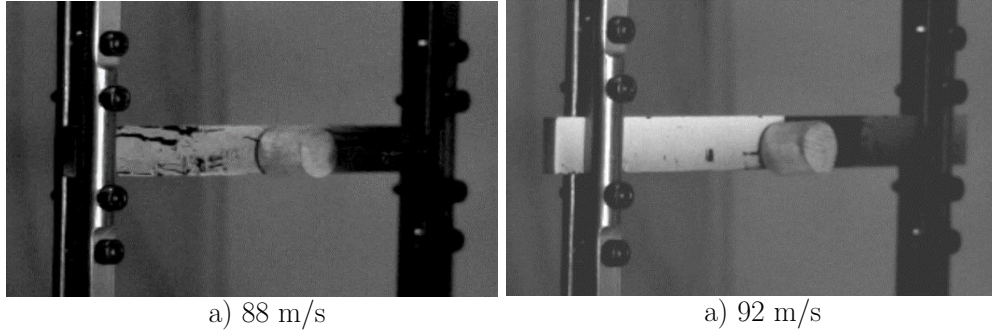


Figure 5: Experimental setup in SBBB test showing the offset of projectile in the impact plane under different impact velocities.

287 centroid of impactor is assumed to coincide with the centroid of the plane of impact
 288 (ii) a section where the actual location of impact from experiments are considered.

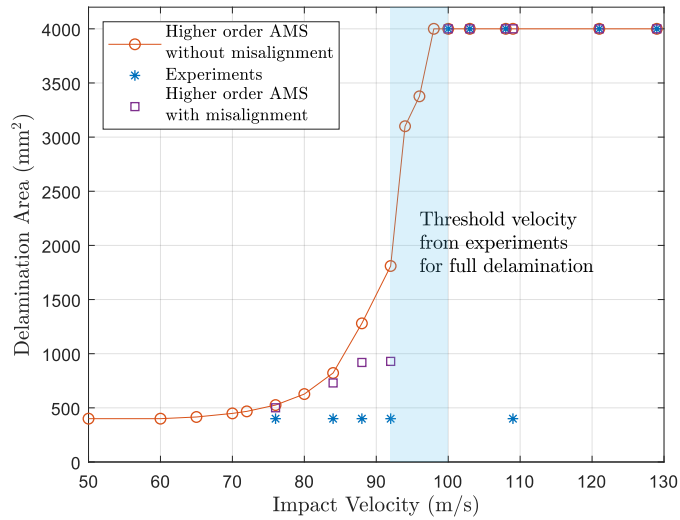


Figure 6: Delamination area obtained for different impact velocities. A mesh size of 1 mm was used for all models.

Table 2: Misalignment details of the projectile at various impact velocities

Impact velocity (m/s)	76	84	88	92	100	103	108	121
offset in the x -direction (mm)	4.2	3.2	1.2	1.3	0.7	0.9	5.8	2.9
offset in the y -direction (mm)	0.0	5.0	0.9	3.3	0.0	0.4	1.7	0.0

289 *4.2.1. Without Eccentricity*

290 The threshold velocity is calculated numerically by varying the impact velocity at
 291 an interval of 4 m/s and is plotted in Figure 6. A cohesive element is considered to
 292 have failed when all the integration points have reached a damage variable equal to
 293 1 (0 - no failure; 1- full failure). At this point, traction is not generated across the
 294 cracked surfaces and they can slide past each other. However, the interpenetration
 295 is avoided due to the presence of a penalty stiffness.

296 From the experiments, it was found that specimens reached full delamination when
 297 the impact velocity was more than 100 m/s. Similar behaviour has also been found
 298 using higher order AMS. When subjected to 98 m/s, the delamination has traversed
 299 along the entire length of the specimen from the pre-defined crack.

300 Also, a stable crack growth is obtained when subjected to velocities slightly lower
 301 than the threshold velocity. The delamination growth at different time increments
 302 when subjected to an impact velocity of 88 m/s, is shown in Figure 7. The cross-
 303 sectional view (x - z plane) of the numerical model is shown along with the damage
 304 plot in the plane of impact (mid-plane through the thickness). The damage growth
 305 increases with the time and maximum damage is attained at 0.3 ms.

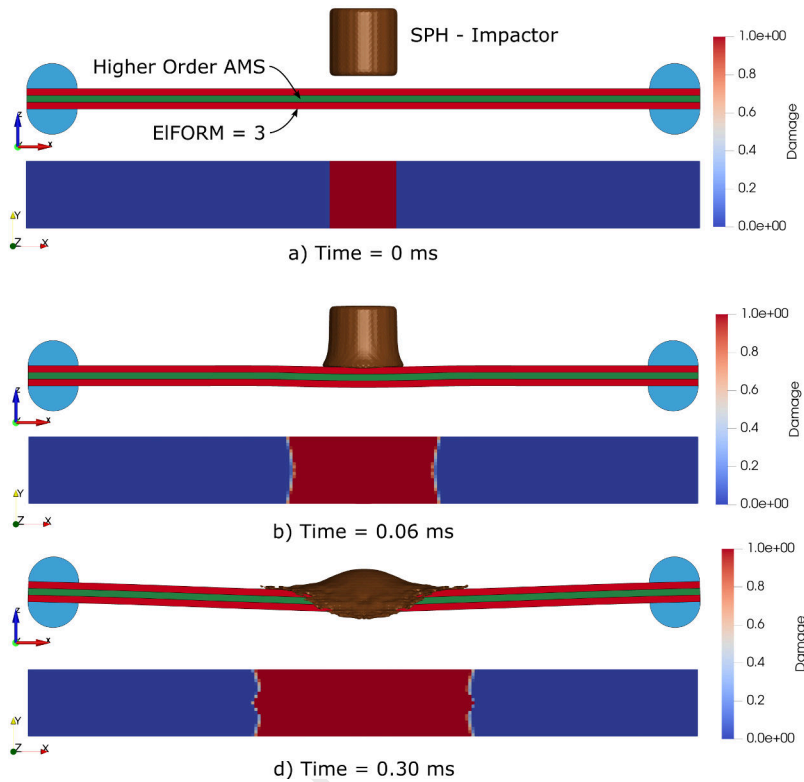


Figure 7: Damage progression in SBBB test specimen subjected to an initial velocity of 88 m/s. The damage growth has stopped at 0.3 ms. (Mesh size 1 mm.)

306 *4.2.2. With Eccentricity*

307 In the experiments, an offset of the projectile in the plane of impact (x - y plane)
 308 can occur, as shown in Figure 5, and it results in a change in the contact area
 309 (offset in x -direction) as well as the loss of symmetry (offset in y -direction). This
 310 can cause a change in the local stress state and the delamination propagation. A
 311 careful investigation of high speed camera images revealed the magnitude of offsets
 312 and they are listed in Table 2.

313 The threshold velocity calculations were repeated for the updated impact locations
 314 and the results are plotted in Figure 6. The threshold velocity remains similar when

Table 3: Calculation of delamination area using different mesh sizes with linear elements and Higher order AMS at an impact velocity of 88 m/s. The values obtained with Higher order AMS are shown in bold and within parentheses.

Mesh size in-plane(x)			0.5 mm	1.0 mm	1.5 mm	2 mm
Number of Elements			400	200	133	100
Through	1.0 mm	6	1480	1202 (1450)	702 (1346)	435 (984)
thickness	0.75 mm	8	1460	1119 (1330)	580 (1380)	439 (905)
direction	0.6 mm	10	1460	939 (1319)	522 (1382)	441 (1038)
(z)	0.5 mm	12	1340	1090 (1290)	489 (1385)	447 (1060)

315 compared to numerical models without offset, but there is a significant reduction in
316 the delamination area for impact velocities slightly lower than the threshold velocity.
317 Also, it can be seen that an offset in the y -direction cause a considerable change in
318 the area of delamination when compared to the offset in x-direction. It is primarily
319 due to the change in the contact area of the projectile.

320 The assumption to perform numerical modelling in the absence of matrix cracks did
321 not appear to have a quantitative influence on the results. The presence of a pre-
322 existing crack, located between two zero degree plies, in this test method initiates
323 delamination, based on the impact velocity, and the energy is dissipated by the
324 delamination growth.

325 4.3. Comparison with Linear Elements

326 To compare the computational benefits obtained with Higher order AMS over linear
327 elements, the SBBB test with an impact velocity of 88 m/s is chosen; linear elements
328 available in LS-DYNA are used for the comparison. The numerical models are anal-

Table 4: Number of degrees of freedom (DOF) required to achieve convergence in the delamination area.

	Mesh size			No. of elements	No. of DOF	Reduction in computational cost
	x	y	z			
Linear elements	0.5	0.5	1.0	96000	288000	-
Higher order AMS	1.5	1.5	1.0	10374	62444	65 %

329 ysed with varying number of elements or mesh size in the in-plane (x and y) and the
 330 through thickness direction (z), as shown in Table 3, and their delamination areas
 331 are calculated; Higher order AMS values are shown within parentheses.

332 To understand the rate of convergence obtained with both set of numerical models, a
 333 third numerical model with a highly refined mesh of 0.25 mm in the x and y-direction
 334 and 0.5 mm in the z-direction is generated using linear elements. This model is
 335 taken as the benchmark to study the rate of convergence with the delamination
 336 area obtained being 1340 mm²; the rate of convergence is higher, if an element
 337 formulation approaches this value with fewer degrees of freedom. The curvature
 338 change around the impact location requires higher number of degrees of freedom to
 339 calculate displacements and tractions than quasi-static benchmark cases.

340 It can be observed from Table 3 that the Higher order AMS approached the bench-
 341 mark value with an in-plane mesh size of 1.5 mm. By contrast the coarsest in plane
 342 mesh with linear elements that approached the benchmark value was 0.5mm. Also,
 343 consistent results are obtained for different AMS mesh sizes in the z-direction. Based
 344 on the data in Table 4, one can see that Higher order AMS requires 4.6 times fewer
 345 number of degrees of freedom than linear elements.

346 To perform the comparison in computational cost, linear elements were also imple-
347 mented as user defined elements. The two modelling methods, implemented as user
348 defined elements and shown in Table 4, were analysed using a high performance clus-
349 ter node with 16 CPUs and a 65 % reduction in computational cost was obtained by
350 using Higher order AMS over linear elements.

351 **5. Conclusions**

352 A novel cohesive element formulation for delamination in a composite specimen has
353 been applied to the case of dynamic loading due to impact. By using this element,
354 fine mesh requirement associated with linear cohesive elements can be alleviated,
355 retaining the essential crack tip driving mechanisms and thus not compromising
356 model accuracy. The presence of additional degrees of freedom gives a C^1 continuity
357 in the cohesive element and helps to solve problems with considerably fewer degrees of
358 freedom. Additionally, Adaptive Mesh Segmentation (AMS) is included to introduce
359 cohesive elements ‘on-the fly’, which eliminates the pre-processing steps required to
360 introduce those elements.

361 The element formulation was validated against experimental results from SBBB tests,
362 which allowed for replication of the stress state inside a specimen without the spu-
363 rious stress induced by boundary conditions. Threshold velocity calculations from
364 numerical models agreed well with the experimental data. Damage growth was also
365 investigated for the eccentricities observed in the experiments in regard to impact
366 location. It was observed that , in both experiment and models, while eccentricities
367 resulted in a change in the damage growth below the threshold energy level, the
368 effect of eccentricity is minimal after crossing the threshold energy.

369 This method could be extended in the future to model in-plane failure behaviour of
370 composite specimens via incorporating continuum damage mechanics methods. Such

371 an integrated method, along with the improvements in computational efficiency pave
372 the way for a general capability to accurately model failure of large scale composite
373 structures with the correct driving mechanisms and coarser meshes thus improving
374 the capability for virtual testing of composites.

375 **Acknowledgements**

376 This work was supported by the Engineering and Physical Sciences Research Council
377 (EPSRC) through the Centre for Doctoral Training in Advanced Composites at the
378 University of Bristol (Grant no. EP/L016028/1). The authors would also like to ac-
379 knowledge Rolls-Royce plc for their support of this research through the Composites
380 University Technology Centre (UTC) at the University of Bristol.

- [1] J. P. Hou, N. Petrinic, C. Ruiz, A delamination criterion for laminated composites under low-velocity impact, *Composites Science and Technology* 61 (14) (2001) 2069–2074. doi:10.1016/S0266-3538(01)00128-2.
- [2] S. Guinard, O. Allix, D. Guédra-Degeorges, A. Vinet, A 3D damage analysis of low-velocity impacts on laminated composites, *Composites Science and Technology* 62 (4) (2002) 585–589. doi:10.1016/S0266-3538(01)00153-1.
- [3] M. R. Wisnom, The role of delamination in failure of fibre-reinforced composites, *Philosophical Transactions of the Royal Society A: Mathematical, Physical and Engineering Sciences* 370 (1965) (2012) 1850–1870. doi:10.1098/rsta.2011.0441.
- [4] O. Allix, P. Ladevèze, Interlaminar interface modelling for the prediction of delamination, *Composite Structures* 22 (4) (1992) 235–242. doi:10.1016/0263-8223(92)90060-P.

- [5] W. G. Jiang, S. R. Hallett, B. G. Green, M. R. Wisnom, A concise interface constitutive law for analysis of delamination and splitting in composite materials and its application to scaled notched tensile specimens, *International Journal for Numerical Methods in Engineering* 69 (9) (2007) 1982–1995. doi:10.1002/nme.1842.
- [6] A. Turon, C. G. Dávila, P. P. Camanho, J. Costa, An engineering solution for mesh size effects in the simulation of delamination using cohesive zone models, *Engineering Fracture Mechanics* 74 (10) (2007) 1665–1682. doi:10.1016/j.engfracmech.2006.08.025.
- [7] R. de Borst, J. J. Remmers, A. Needleman, Mesh-independent discrete numerical representations of cohesive-zone models (jan 2006). doi:10.1016/j.engfracmech.2005.05.007.
- [8] P. W. Harper, S. R. Hallett, Cohesive zone length in numerical simulations of composite delamination, *Engineering Fracture Mechanics* 75 (16) (2008) 4774–4792. doi:10.1016/j.engfracmech.2008.06.004.
- [9] R. Krueger, Virtual crack closure technique: History, approach, and applications, *Applied Mechanics Reviews* 57 (2) (2004) 109–143. doi:10.1115/1.1595677.
- [10] A. Tabiei, W. Zhang, Composite Laminate Delamination Simulation and Experiment: A Review of Recent Development, *Applied Mechanics Reviews* 70 (3), 030801 (06 2018). doi:10.1115/1.4040448.
- [11] E. Pietropaoli, A. Riccio, On the robustness of finite element procedures based on virtual crack closure technique and fail release approach for delamination growth phenomena. definition and assessment of a novel method-

- ology, *Composites Science and Technology* 70 (8) (2010) 1288 – 1300. doi:10.1016/j.compscitech.2010.04.006.
- [12] N. Moës, T. Belytschko, Extended finite element method for cohesive crack growth, *Engineering Fracture Mechanics* 69 (7) (2002) 813–833. doi:10.1016/S0013-7944(01)00128-X.
- [13] J. M. Melenk, I. Babuška, The partition of unity finite element method: Basic theory and applications, *Computer Methods in Applied Mechanics and Engineering* 139 (1-4) (1996) 289–314. doi:10.1016/S0045-7825(96)01087-0.
- [14] A. Hansbo, P. Hansbo, A finite element method for the simulation of strong and weak discontinuities in solid mechanics, *Computer Methods in Applied Mechanics and Engineering* 193 (33-35) (2004) 3523–3540. doi:10.1016/j.cma.2003.12.041.
- [15] B. Y. Chen, S. T. Pinho, N. V. De Carvalho, P. M. Baiz, T. E. Tay, A floating node method for the modelling of discontinuities in composites, *Engineering Fracture Mechanics* 127 (2014) 104–134. doi:10.1016/j.engfracmech.2014.05.018.
- [16] L. F. Kawashita, A. Bedos, S. R. Hallett, Modelling Mesh Independent Transverse Cracks in Laminated Composites with a Simplified Cohesive Segment Method, *Tech. Rep. 2* (2012).
- [17] T. Belytschko, W. Liu, B. Moran, *Nonlinear Finite Elements for Continua and Structures*, John Wiley & Sons, Ltd, 2000.
- [18] J. Selvaraj, S. Mukhopadhyay, L. F. Kawashita, S. R. Hallett, Modelling delaminations using adaptive cohesive segments with rotations in dy-

dynamic explicit analysis, *Engineering Fracture Mechanics* 245 (2021) 107571. doi:<https://doi.org/10.1016/j.engfracmech.2021.107571>.

- [19] J. Selvaraj, L. Kawashita, G. Allegri, S. Hallett, Adaptive Mesh Segmentation for Modelling Dynamic Delamination Initiation and Propagation in Thick Composite Laminates, in: 12th European LS-DYNA conference, 2019.
- [20] T. Menouillard, T. Belytschko, Smoothed nodal forces for improved dynamic crack propagation modeling in XFEM, *International Journal for Numerical Methods in Engineering* 84 (1) (2010) 47–72. doi:[10.1002/nme.2882](https://doi.org/10.1002/nme.2882).
- [21] S. R. Hallett, Three-point beam impact tests on T300/914 carbon-fibre composites, *Composites Science and Technology* 60 (1) (2000) 115–124. doi:[10.1016/S0266-3538\(99\)00099-8](https://doi.org/10.1016/S0266-3538(99)00099-8).
- [22] L. Greve, A. K. Pickett, Delamination testing and modelling for composite crash simulation, *Composites Science and Technology* 66 (6) (2006) 816–826. doi:[10.1016/j.compscitech.2004.12.042](https://doi.org/10.1016/j.compscitech.2004.12.042).
- [23] S Read, inventor; Rolls-Royce PLC, assignee, Test apparatus and method of testing. US 7,845,207 B2 (Dec. 2010).
- [24] G. Mohamed, G. Kalwak, S. R. Hallett, M. Jevons, Modelling soft body impact of through-thickness reinforced composites, in: 16th European Conference on Composite Materials, Seville, Spain, 2014.
- [25] Y. M. Le Cahain, J. Noden, S. R. Hallett, Effect of insert material on artificial delamination performance in composite laminates, *Journal of Composite Materials* 49 (21) (2015) 2589–2597. doi:[10.1177/0021998314550428](https://doi.org/10.1177/0021998314550428).

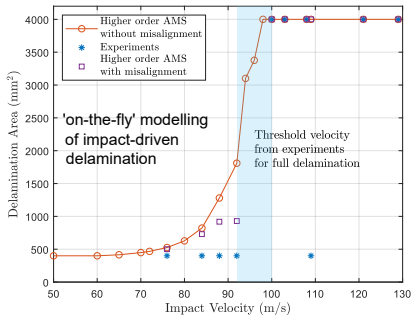
- [26] S. M. Yunus, T. P. Pawlak, R. D. Cook, Solid elements with rotational degrees of freedom: Part 1 hexahedron elements, *International Journal for Numerical Methods in Engineering* 31 (3) (1991) 573–592. doi:10.1002/nme.1620310310.
- [27] C. J. Shepherd, G. J. Appleby-Thomas, P. J. Hazell, D. F. Allsop, The dynamic behaviour of ballistic gelatin, in: *AIP Conference Proceedings*, Vol. 1195, 2009, pp. 1399–1402. doi:10.1063/1.3295071.
- [28] Y. Zhou, Y. Wang, Y. Xia, S. Jeelani, Tensile behavior of carbon fiber bundles at different strain rates, *Materials Letters* 64 (3) (2010) 246 – 248. doi:https://doi.org/10.1016/j.matlet.2009.10.045.
- [29] N. Taniguchi, T. Nishiwaki, H. Kawada, Tensile strength of unidirectional cfrp laminate under high strain rate, *Advanced Composite Materials* 16 (2) (2007) 167–180. doi:10.1163/156855107780918937.
- [30] M. Yasaei, G. Mohamed, A. Pellegrino, N. Petrinic, S. R. Hallett, Strain rate dependence of mode ii delamination resistance in through thickness reinforced laminated composites, *International Journal of Impact Engineering* 107 (2017) 1 – 11. doi:https://doi.org/10.1016/j.ijimpeng.2017.05.003.
- [31] H. Cui, Y. Mahadik, S. R. Hallett, I. K. Partridge, G. Allegri, S. A. Ponnusami, N. Petrinic, Coupon scale z-pinned im7/8552 delamination tests under dynamic loading, *Composites Part A: Applied Science and Manufacturing* 125 (2019) 105565. doi:https://doi.org/10.1016/j.compositesa.2019.105565.

Soft Body Impact on Composites: Delamination experiments and Advanced Numerical Modelling

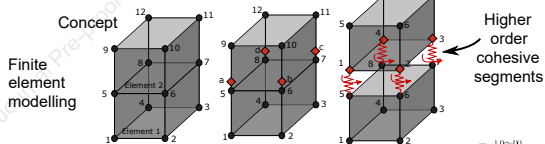
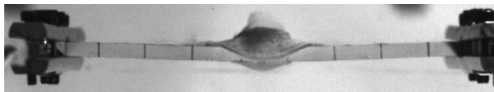
A research article entitled 'Soft Body Impact on Composites: Delamination experiments and Advanced Numerical Modelling' is submitted for consideration by Composites Science and Technology. We confirm that the work has not been submitted for publication nor has it been published in any other journal.

CREDIT author contribution

Jagan Selvaraj	Conceptualisation, Methodology, Software, Validation, Investigation, Writing – Original draft
Luiz. F. Kawashita	Conceptualisation, Methodology, Software, Writing – Review & Editing, Supervision
Mehdi Yasaee	Validation, Formal Analysis, Investigation
Gordon Kalwak	Methodology, Validation, Investigation
Stephen. R. Hallett	Conceptualisation, Resources, Writing – Review and Editing, Supervision, Project administration, Funding acquisition



with 4.5 times fewer degrees of freedom than linear elements



2021-03-20

Soft body impact on composites: delamination experiments and advanced numerical modelling

Selvaraj, Jagan

Elsevier

Selvaraj J, Kawashita LF, Yasae M, et al., (2021) Soft body impact on composites: delamination experiments and advanced numerical modelling. *Composites Science and Technology*, Volume 208, May 2021, Article number 108777

<https://doi.org/10.1016/j.compscitech.2021.108777>

Downloaded from Cranfield Library Services E-Repository